Journal of Applied Polymer Science

Bonding performance and fracture morphology of a hybrid multiscale epoxy adhesive on oil-covered substrates

Zhongwei Zhang, Yefa Tan, Xiaolong Wang, Hua Tan, Xiang Hong
College of Field Engineering, PLA University of Science and Technology, Nanjing 210007, China
Correspondence to: Y. Tan (E-mail: tanyefa7651@163.com or zhangzhongwei.cn@gmail.com)

ABSTRACT: A hybrid multiscale epoxy adhesive reinforced with a combination of short carbon fibers and rubber nanoparticles was prepared for bonding oil-covered aluminum substrates. The shear performance of the bonded joints was investigated as a function of the oil layer thickness. Scanning electron microscopy and energy-dispersive X-ray analysis studies were carried out to evaluate the oil-diffusion behavior near the substrate–adhesive interface. The results show that the shear strength decreased, whereas the distribution range of the testing results increased as the oil layer thickness increased. When the oil layer was thinner than 10 μm, the oil-accommodating adhesive could be used directly without degreasing, whereas over 96% of the bonding strength could be retained with almost no change in the failure probability. The analysis of Weibull distribution indicated that the shear strength and Weibull modulus were 18.89 MPa and 13.503, respectively. By analyzing the relationship between the shear strength results and the failure model of the fracture surface, we found a correlation. © 2015 Wiley Periodicals, Inc. J. Appl. Polym. Sci. **2016**, *133*, 42898.

KEYWORDS: adhesives; applications; mechanical properties; morphology; resins

Received 6 July 2015; accepted 29 August 2015
DOI: 10.1002/app.42898

INTRODUCTION

Adhesively bonded joints are considered viable alternatives to traditional joint methods in engineering areas, and they show numerous advantages, including a as higher strength-to-weight ratio, a lower stress concentration, and a longer service life. Thus, they have been widely used in automobile production, aircraft manufacturing, and engineering repairs.[1–7] In some application situations, the oil covered on the substrate surface usually brings inconvenience to the processing procedure. For example, in the automobile industry, many part surfaces are covered with a thin layer of oil because of the machining process or for anticorrosion purposes. However, a clean surface without oil is generally considered a basic requirement for reliable bonding. So, the degreasing process is necessary before adhesive bonding; this is always undesirable because it means additional manpower, special equipment, and a higher cost. Moreover, in the field of oil transportation, leaked oil pipelines need to be repaired immediately. To guarantee a reliable repair quality, the degreasing process should be adopted before repair because the damaged location of oil pipelines is usually covered by a layer of oil. However, this additional degreasing process usually decreased the efficiency of rush repair sharply; this hampers the development of rush repair technology in the field environment.

To improve efficiency and reduce costs, oil-accommodating adhesives have been developed for such requirements. Ogawa and Hongo[8] investigated the oil-absorption behavior and determined the saturated oil concentration of a hybrid oil-accommodating adhesive. Debski *et al.*[9] evaluated the ability of a hybrid adhesive to produce durable metal–metal bonds without previous cleaning of the oil contaminants from the substrate. Hong and Boerio[10] studied the mechanical performance of an amidoamine-cured hybrid epoxy adhesive on the clean and oil-contaminated electrogalvanized steel. However, the inclusion of fillers into hybrid adhesive systems in previous studies has modified or adjusted some properties of the adhesives at the expense of other important properties. For instance, the inclusion of nitrile–butadiene rubber enhanced the T-peel and shear strengths for both degreased and oiled steel plates but sharply reduced the tensile strength of the cured adhesive. When the nitrile–butadiene rubber content reached 25 wt %, the tensile strength of the cured adhesive decreased by over 40% compared to that of the unfilled samples.[8]

To improve the comprehensive performance of a hybrid material system without the sacrifice of other key properties, a promising method is the fabrication of hybrid multiscale material systems reinforced with both microsized and nanosized reinforcements. Recent studies have indicated that the multiscale fillers contribute to the improvement of the overall properties of epoxy systems. Tang *et al.*[11] reported that the combined use of multiscale rubber particles not only provided superior efficiency in enhancing the

impact resistance but also resulted in a balanced glass-transition temperature in the epoxy composites. Zhang and coworkers[12,13] found that the multiscale carbon fillers led to significant synergy in the tensile and fracture mechanical properties of the epoxy resin. Other studies on hybrid multiscale epoxy composites can be found in the literature.[14–18] Although notable achievements of multiscale materials have been attained, little attention has been paid to the mechanical performance of the hybrid multiscale epoxy adhesives on oil-covered substrates. Among the many kinds of reinforcements, the short carbon fibers (SCFs) contribute to simultaneously enhancing the modulus and impact strength of the epoxy because of their large length-to-radius ratio and high specific strength.[19–21] Moreover, the proper addition content of rubber nanoparticles (RNPs) causes notable improvements in the peel strength and fracture toughness of the cured adhesives.[22] In particular, as a kind of vulcanized nitrile rubber, RNPs have some capability for absorbing oil.[23] Therefore, in our study, the epoxy resin was adopted as the matrix for fabricating a hybrid oil-accommodating adhesive reinforced with a combination of SCFs and RNPs.

In this study, the bonding performance of a hybrid multiscale oil-accommodating adhesive was investigated by way of shear strength testing. The influence of the oil layer thickness on the shear strength, failure probability, and fracture surface morphology was also studied. Scanning electron microscopy (SEM) was used to observe the effect of oil absorption on the cross-sectional microstructure and fracture morphology. Energy-dispersive X-ray analysis (EDAX) was used to study the diffusion behavior of oil in the bonding layer. Weibull analysis was adopted to investigate the variation trend of the shear strength distribution as the oil layer thickness increased.

EXPERIMENTAL

Materials

Bisphenol A epoxy resin (WSR618), purchased from Bluestar Wuxi Petrochemical Co., Ltd. (China), was used as the matrix. A commercial hardener (FS-2B), produced by Chuzhou Hui-Sheng Electronic Materials Co., Ltd. (China), was used as the curing agent with a mixing weight ratio to WSR618 of 1:1. RNPs (Narpow VP-501) were nitrile–butadiene rubber particles with a diameter of about 100 nm; these were kindly provided by SINOPEC Beijing Research Institute of Chemical Industry (China). SCFs were T700SC-12000-50C from Toray Co., Ltd. (Japan); they were chopped into pieces 3 mm in length. The oil and coupling agent were dimethyl silicon oil and KH550 from Wells Electronic Materials Co., Ltd. (China), respectively.

Preparation of the Hybrid Multiscale Adhesive

To obtain a highly dispersed system, both the epoxy resin and the curing agent were filled with reinforcements, and the epoxy-based blends and curing agent blends were marked as parts A and B, respectively. An example of the preparation process of part A follows. First, the SCFs were surface-desized in a Soxhlet extractor for 72 h with acetone as the extraction medium. Then, the SCFs, RNPs, and coupling agent were immersed into the epoxy system. After that, the blend was processed by a planetary ball mill (QM-ISP4, Nanjing University Instrument Plant, China) in the vacuum milling pot. The ball-milling process can result in high shear forces, which can effectively break up the agglomerates of fillers in the epoxy system. Finally, the blend was processed by ultrasonic treatment at 60°C for 2 h. The addition contents of epoxy resin, RNPs, coupling agent, and SCFs were 100, 6, 2, and 1–6 phr, respectively. The preparation procedure of part B was the same as that of part A.

Table I. Drops of the Oil–Acetone Solution Needed to Prepare a Specific Oil Layer Thickness

Thickness of the oil layer (μm)	0	1	2	3	4	5	6	7	8
Drops of oil–acetone solution	—	45	89	134	179	223	268	313	357

Preparation of Bonded Joints

The two-part adhesive was mixed and placed in the vacuum chamber for about 2 min to release air bubbles. The substrates were superposed and bonded to a configuration according to ASTM D 1002-10 standard with aluminum sheets. This configuration was a suitable selection as it has been proven simple to make, and it involves different stress condition modes in the shear direction.[24] The bonding layer thickness could be controlled by changes in the additional pressure on the joint.[25] The samples were then cured at room temperature for 24 h before testing.

Control Method of the Oil Layer Thickness

To investigate the influence of oil layer thickness on the bonding performance of the oil-covered substrates, the following process was adopted to obtain a precise value of oil layer thickness. First, an injector with a volume of 1 mL was filled with oil, and a free-falling droplet dropped down by the slow pushing of the pushrod at room temperature. According to the number of oil droplets and their total volume, the volume of each droplet was calculated. Second, an oil–acetone solution was obtained by the dissolution of 10 drops of oil in 1 mL of acetone. The volume of each oil–acetone solution droplet was calculated with the same method as discussed previously. In our study, the size of the shear area was 25.4 × 12.7 mm^2. Therefore, when a drop of oil–acetone solution was uniformly distributed on the shear area, its theoretical thickness should have been 0.0224 μm after the acetone was volatilized. Table I indicates corresponding drops of oil–acetone solution with different oil layer thicknesses.

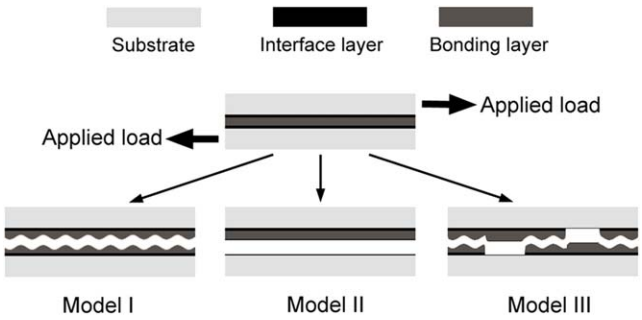

Figure 1. Schematic description of the failure models.

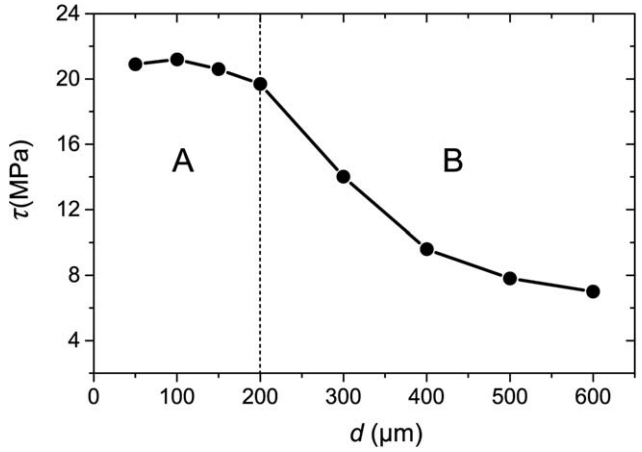

Figure 2. Curve of the dependence of the shear strength (τ) on the thickness of the bonding layer (d).

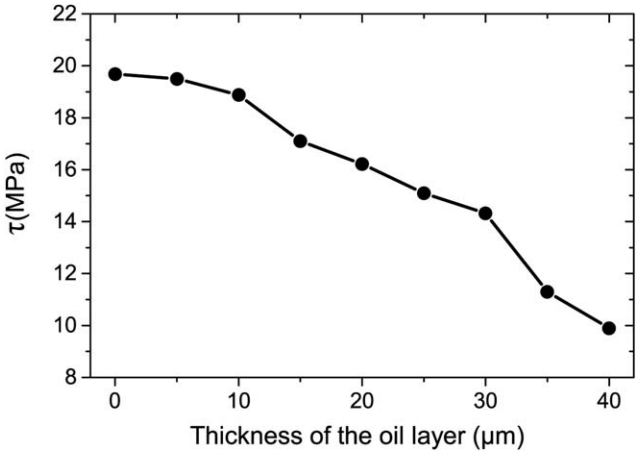

Figure 4. Curve of the dependence of the shear strength (τ) on the thickness of the oil layer.

Characterization

The shear strength was tested on a SANS CMT5105 universal testing machine at room temperature at a speed of 1.3 mm/min. At least 20 specimens were tested for each category.

SEM (FEI-QUANTA200, United States) was used to examine the cross-sectional morphologies of the specimens. The elemental distribution was analyzed by EDAX (FEI-QUANTA200).

In general, three failure models are considered for bonded specimens, as shown in Figure 1. When the bonded specimens ruptured in the bonding layer in terms of model I (cohesive failure model), remaining adhesive existed on both of the substrate surfaces. However, when the specimens ruptured on the interface layer in terms of model II (interface failure model), remaining adhesive only existed on one of the two substrate surfaces. Actually, a mixture failure model including both models I and II, that is, model III, was proven to play a dominant role in the ruptured specimens. To further study the fracture morphology and its relationship to the shear strength results of the oil-covered bonded specimens, an easy procedure was adopted as follows. First, photographs of the fracture surface were taken by a Nikon D90 camera and then opened in the image processing software Image-Pro Plus 6.0. Second, the failure areas were selected. Then, the Count/Size menu commands were used to select colors that defined the remaining adhesive on the fracture surface. Third, the PerArea command was used to calculate the area ratio of the remaining adhesive to the selected rectangular regions. As a result, the following equations could be obtained:

$$\begin{cases} x+y_A=a \\ x+y_B=b \\ x+y_A=y_B=1 \end{cases} \quad (1)$$

where x represents the area ratio of remaining adhesive attributed to model I; y_A and y_B are the area ratios of the remaining adhesive on substrates A and B attributed to model II, respectively; and a and b are the measured area ratios of remaining adhesive to the selected rectangular regions. On the basis of eq. (1), the area ratio of models I and II to the selected rectangular regions were obtained in terms of x and $y_A + y_B$, respectively.

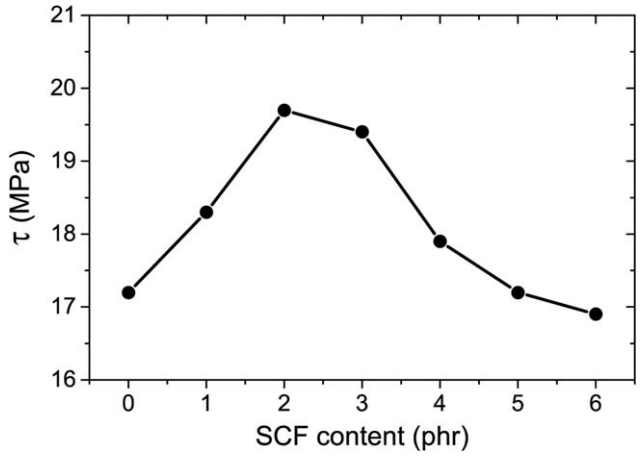

Figure 3. Curve of the dependence of the shear strength (τ) on the SCF content.

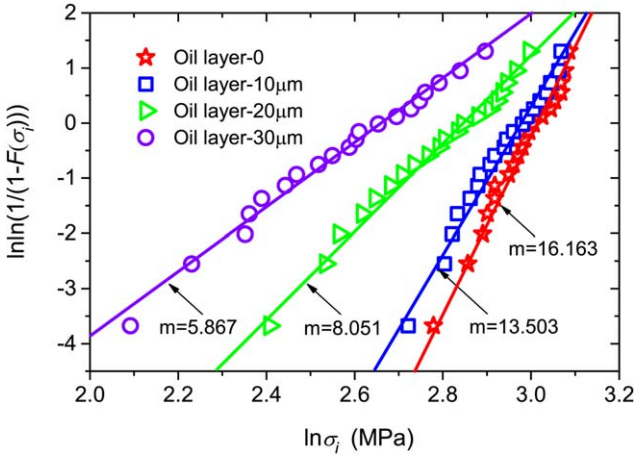

Figure 5. Weibull plot for the bonded specimens. [Color figure can be viewed in the online issue, which is available at wileyonlinelibrary.com.]

Table II. Weibull Data for the Tensile Shear Tests

Thickness of the oil layer (μm)	m	Shear strength (MPa)			Standard deviation (MPa)
		Mean	Maximum	Minimum	
0	16.163	19.68	21.90	16.10	1.58
10	13.503	18.89	21.51	15.18	1.77
20	8.051	16.22	20.06	11.13	2.50
30	5.867	14.32	20.08	7.14	3.65

RESULTS AND DISCUSSION

Results of the Shear Strength Tests

Figure 2 shows the plot of the shear strength as a function of the bonding layer thickness in the range 50–600 μm in which the SCF content was 2 phr. This curve was divided into two zones. The bonding layer thickness in zone A was less than 200 μm, where the shear strength first increased and then decreased with increasing bonding layer thickness. All of the results in zone A remained around 20 MPa. The shear strength achieved a maximum value of 21.2 MPa at a bonding layer thickness of 100 μm. Comparatively, zone B covered the range of bonding layer thicknesses from 200 to 600 μm, where the shear strength decreased sharply with increasing bonding layer thickness. In practical applications, an extremely thin bonding layer usually needs precise surface treatment; this always means a reduction in the process efficiency and an increase in the cost. To balance the contradiction between the bonding performance and workability in practical use, 200 μm was determined to be the optimal bonding layer thickness. The corresponding result of the shear strength was 19.7 MPa.

The effect of the SCF content on the shear strength is shown in Figure 3, in which the bonding layer thickness was 200 μm. As indicated in the figure, when the SCF content was smaller than 2 phr, the shear strength increased significantly with increasing SCF content. The shear strength achieved a maximum value of 19.7 MPa at an SCF content of 2 phr. If the SCF content increased further, the shear strength decreased. Therefore, 2 phr was considered to be the optimal SCF content.

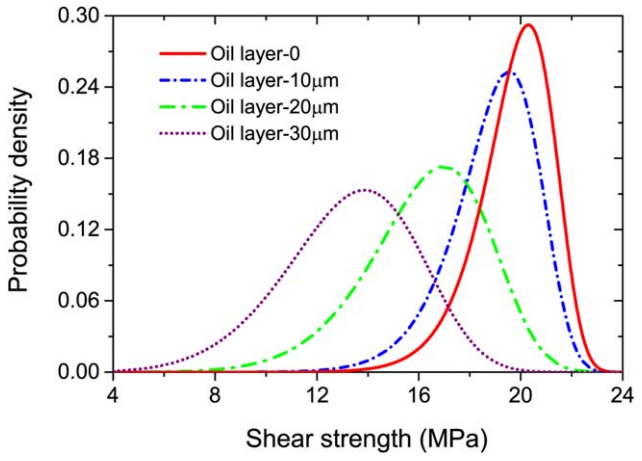

Figure 6. Shear strength distributions based on the Weibull theory. [Color figure can be viewed in the online issue, which is available at wileyonlinelibrary.com.]

Figure 4 illustrates the effect of the oil layer thickness on the shear strength of the oil-covered bonded joints. It shows that the shear strength decreased with increasing oil layer thickness in the whole range. However, when the oil layer was thinner than 10 μm, the shear strength decreased slowly but still remained higher than 18 MPa. The curve presented an almost linear decreasing trend in the oil layer thickness range 15–30 μm. With a further increase in the oil layer thickness, the shear strength decreased sharply. A similar result was found in the published literature,[8] in which a sharp decrease in the T-peel strength was obtained after the sample was soaked in oil.

Analysis of the Weibull Distribution

Because the adhesively bonded joints are potential alternatives to mechanical joints in some engineering fields, a high level of bonding reliability and performance reproducibility are increasingly being required. However, in practical applications, the use of adhesively bonded joints has not yet been proven to be a fully reliable joining methodology.[26,27] Therefore, further work needs to be undertaken to describe and evaluate the statistics of bonding strength. On the basis of the weakest link concept, the Weibull distribution has been reported to be available in the failure probability of bonded joints[28,29] or the analysis of fiber fracture statistics.[30] The Weibull failure probability is given by the following equation:

$$F(\sigma_i)=1-\exp[-(\sigma_i/\sigma_0)^m] \quad (2)$$

where i represents the serial number of the fractured sample, $F(\sigma_i)$ is the failure probability of the number i sample, σ_i is the applied stress, σ_0 is the characteristic stress, and m is the Weibull modulus.

m is considered a measure of the variability of the testing results. A higher value of m indicates a more homogeneous population of the flaw and a better predictability of the testing results. On the contrary, a lower value of m presents a larger distribution range of the testing results and a less predictable failure behavior. Equation (2) can be reformulated as follows:

$$\ln\{\ln[1-F(\sigma_i)]\} = m\ln\ \sigma_i - m\ln\ \sigma_0 \quad (3)$$

It shows a linear relationship between $\ln\{\ln[1-F(\sigma_i)]\}$ and $\ln\ \sigma_i$. Also, the scaling coefficient is m. In this study, the shear performance of the oil-covered bonded joints was studied on the basis of Weibull theory for the first time. First, 20 specimens

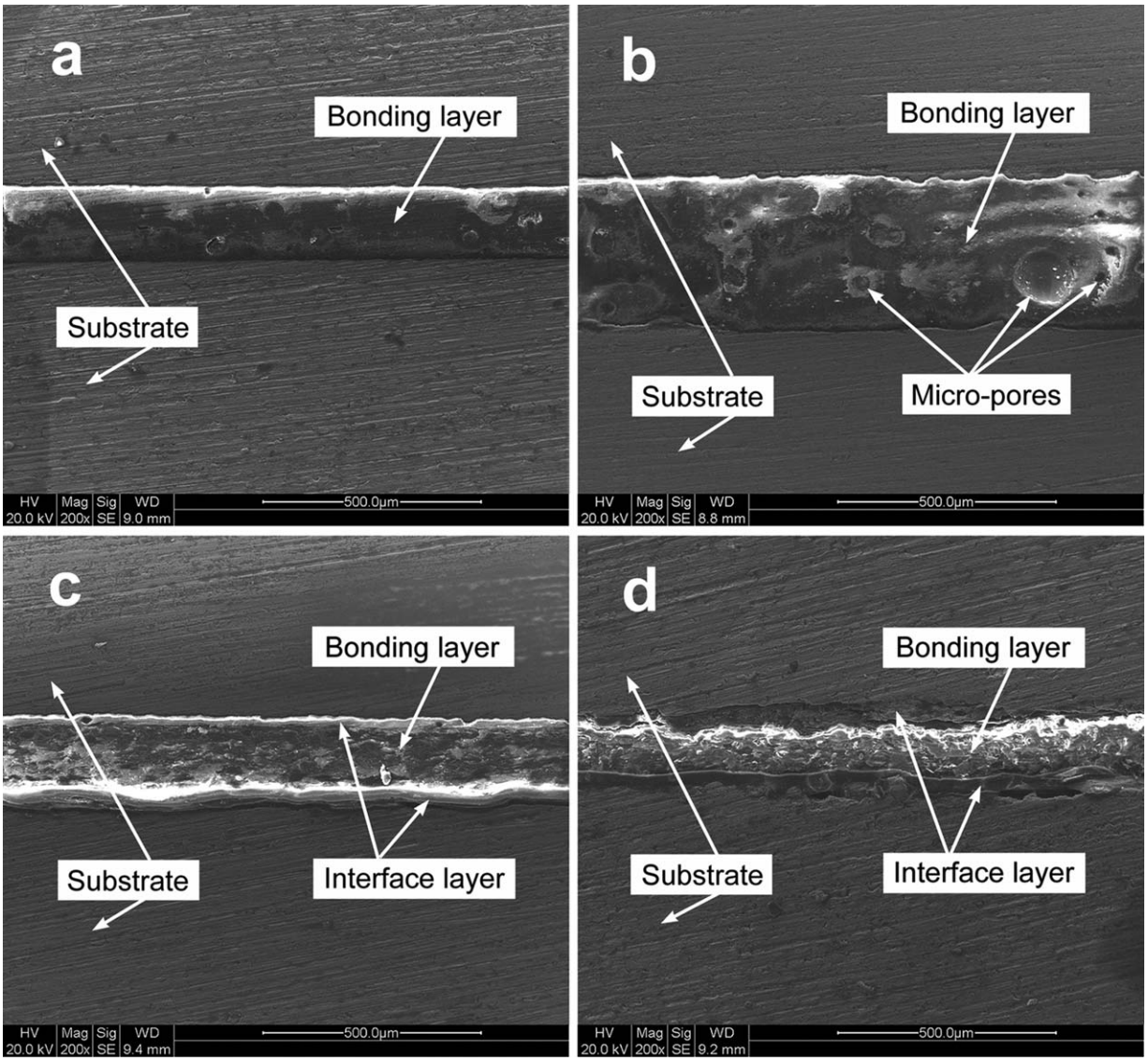

Figure 7. SEM micrographs of the cross-sectional areas: (a) bonding layer of 200 μm and oil-free sample, (b) bonding layer of 400 μm and oil-free sample, (c) oil layer of 20 μm and oil-covered sample, and (d) oil layer of 30 μm and oil-covered sample.

were tested for each category to obtain the testing results of applied stress. Then, these results were ranged from small to large order as follows: $\sigma_1 \leq \sigma_2 \leq \ldots \leq \sigma_i \ \ldots \leq \sigma_N$, where N is the quantity of total specimens. Thus, $F(\sigma_i)$ under an applied stress of σ_i could be expressed with eq. (4). Finally, a least-square method was adopted to analyze the ordinate of ($\ln \sigma_i$, $\ln\{\ln[1 - F(\sigma_i)]\}$):

$$F(\sigma_i) = (i - 0.5)/N \tag{4}$$

Figure 5 shows the Weibull plots for the oil-covered specimens. We observed that almost all of the experimental results were in good agreement with the corresponding best fit lines. M decreased with increasing oil layer thickness. When the oil layer thicknesses were 0, 10, 20, and 30 μm, the corresponding values of m were determined to be 16.163, 13.503, 8.501, and 5.867, respectively. According to the weakest link concept of Weibull theory, the results suggest that an increase in the oil layer thickness would lead to the uneven distribution of flaws in the bonding layer. Therefore, the failure predictability and the performance reproducibility of the bonded joints will become worse. This judgment was also confirmed by the standard deviation of the testing results shown in Table II. For example, the standard deviation of the oil-free specimens was 1.58 MPa. However, for the specimens covered with a 30-μm oil layer, this value was 3.65 MPa; this was an increase of 131%.

Figure 6 illustrates the distribution of failure probability density according to Weibull theory. As shown in the figure, both the maximum probability density and its corresponding shear strength decreased with increasing oil layer thickness, and the shape of the curve tended to be flatter. This shape variation demonstrated a wider dispersion of the testing results. In comparison with the specimens covered with a 20- or 30-μm oil layer, the probability distribution curve of the specimens covered with a 10-μm oil layer was closer to that of the oil-free specimens. This implied that the 10-μm oil layer had less

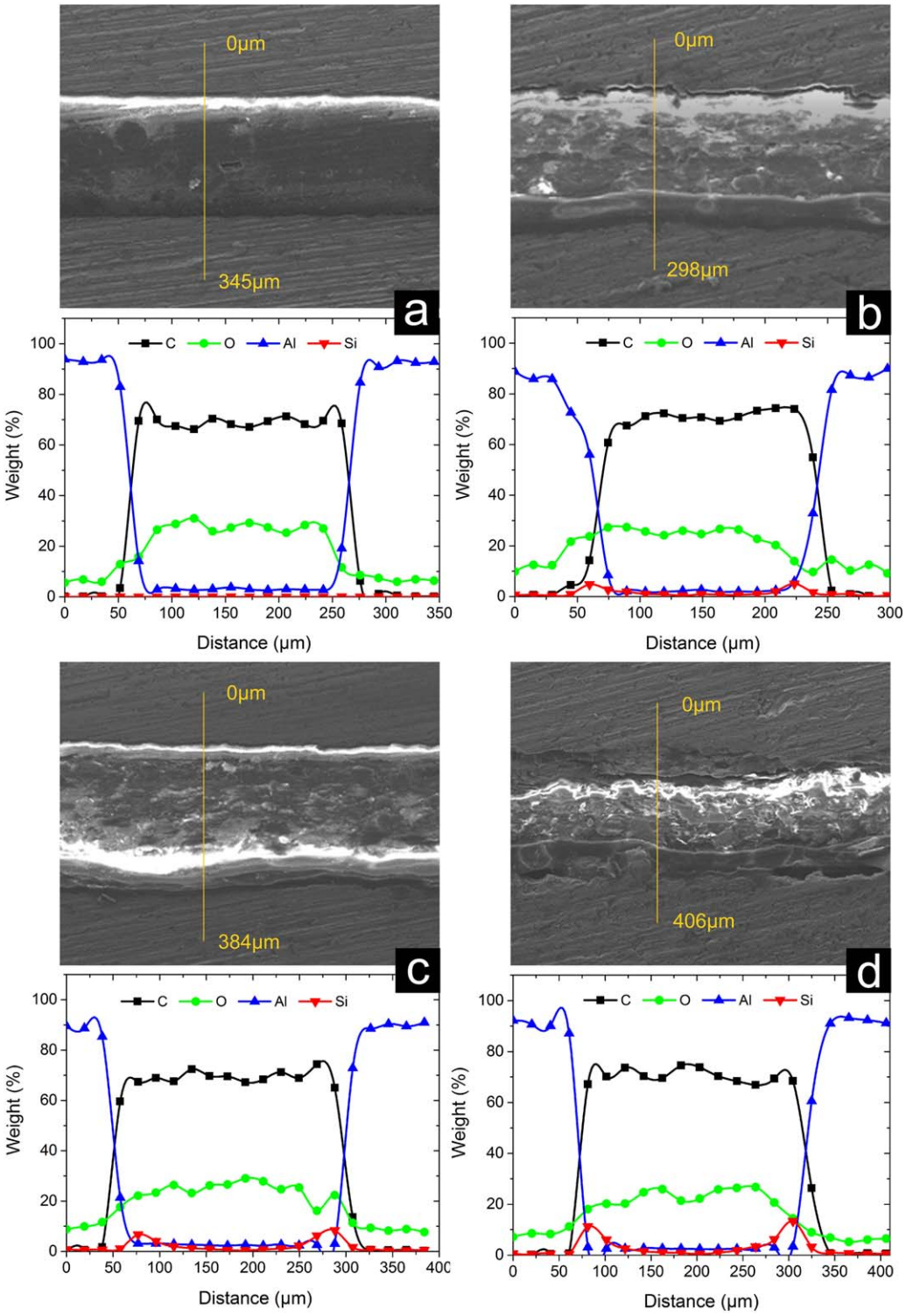

Figure 8. Interface micrographs and elemental distribution curves with different oil layer thicknesses: (a) 0, (b) 10, (c) 20, and (d) 30 μm. [Color figure can be viewed in the online issue, which is available at wileyonlinelibrary.com.]

influence on the shear performance of the bonded joints. This result is in accordance with the findings shown in Figure 4 and indicates that the shear strength only decreased slightly when the oil layer thickness was smaller than 10 μm.

Cross-Sectional Micrographs of the Bonding Layer

Figure 7(a,b) presents SEM micrographs of the cross-sectional areas of the specimens with bonding layer thicknesses of 200 and 400 μm, respectively. It shows that some micropores existed

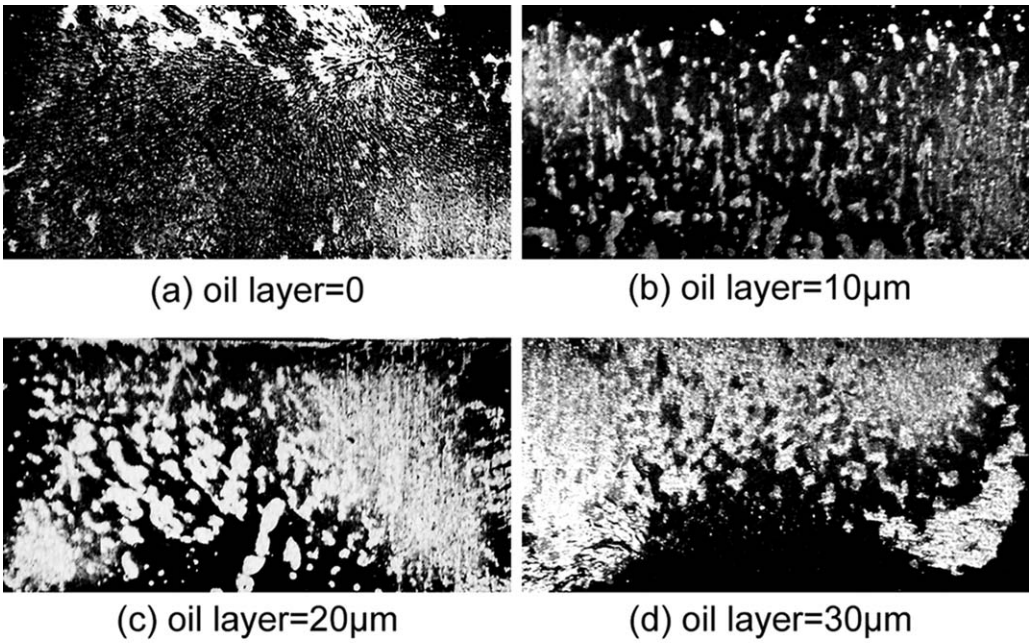

Figure 9. Fracture surfaces with different oil layer thicknesses.

in the cross-sectional area of the specimens with a bonding layer thickness of 400 μm [Figure 7(b)]. These features may have been due to the remaining air bubbles and volume shrinkage during the curing process of the epoxy adhesive. They increased the stress concentration level and reduced the shear strength of the bonding layer. By contrast, few micropores were found on the cross-sectional area of the specimens with a bonding layer thickness of 200 μm [Figure 7(a)]. In this study, the smaller bonding layer thickness indicated that a higher pressure was applied on the specimen, and this led to a shrinkage of the volume of air bubbles. Meanwhile, the microstructure of the bonding layer in Figure 7(a) also indicated a lower stress concentration level and a higher shear strength of the specimen; this was consistent with the results in Figure 2. A similar finding was reported in which an 80 μm thick bonding layer was superior to a 200 μm thick one in shear strength.[25]

Figure 7(c,d) illustrates the effect of the oil layer thickness on the cross-sectional microstructure of the oil-covered specimens. Compared with the oil-free specimens, obvious interfacial features were observed at the substrate–adhesive interface. With the increase in oil layer thickness, more debonding flaws were found at the substrate–adhesive interface; this indicated that the interfacial area may have become the origin of shear failure for the oil-covered bonded joints.

Oil-Diffusion Behavior

SEM micrographs and elemental distribution in the cross section of the oil-covered specimens are presented in Figure 8. As shown in Figure 8(a–d), C, O, Al, and Si were detected as the main components of the composition. As the two major elements of the substrate, the different composition percentages of Al and O in each specimen were attributed to the differences in the oxidation degrees of the aluminum substrate. Because of the chemical durability of oil used in this study [dimethyl silicon oil, $(C_2H_6OSi)_n$], the oil-diffusion behavior was mainly considered as a physical process rather than a chemical process. The dimethyl silicon oil was the only source of Si in this study; thus, the elemental distribution of Si was considered the characterization of oil distribution in the cross-sectional area. As a bisphenol A epoxy resin adhesive, C and O were the major elements. The content variation of C was attributed to the scattered SCFs in the epoxy matrix. The content of C increased when the energy spectrum detected on an SCF but returned to a normal level away from the SCFs; a similar phenomenon was also reported in the published literature.[31] It is noteworthy that no N was detected in this study; this was in contrast with the

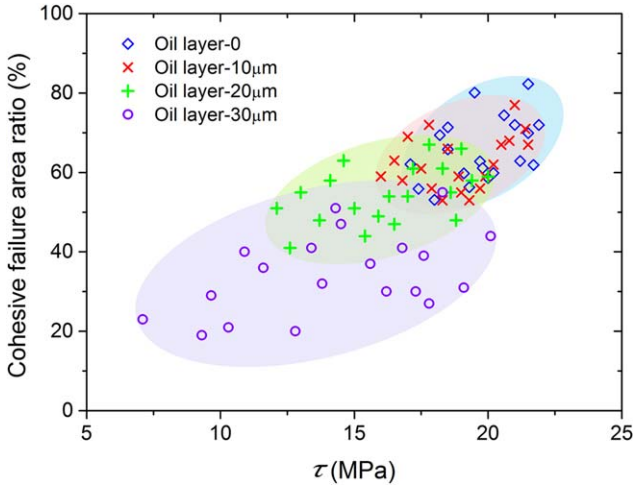

Figure 10. Relationship between the cohesive failure area ratio and the shear strength (τ) with different oil layer thicknesses. [Color figure can be viewed in the online issue, which is available at wileyonlinelibrary.com.]

fact that N should have been one of the composition elements of the curing agent, FS-2B.[32] This phenomenon could be explained from the two following aspects: (1) the epoxy part and the substrate had strong absorption effects on the soft X-rays,[33] and (2) N was not uniformly distributed in the adhesive.

For the oil-free specimen [Figure 8(a)], no obvious interfacial features were observed in the cross-sectional area. The elemental analysis result indicated that no Si was detected in the whole range. For the specimen covered with 10 μm thick oil layer [Figure 8(b)], interface layers with thicknesses of 30–60 μm were found at the substrate–adhesive interface. The elemental analysis results show that the content of Si achieved a maximum value of about 5% and the distribution range was consistent with the thickness of interface layer; this implied that the oil diffused toward the bonding layer for about 20–50 μm during the curing process. When the oil layer thickness increased to 20 μm [Figure 8(c)], some flaws were observed at the substrate–adhesive interface. The distribution range of Si further increased to 80–100 μm; this indicated that the oil would diffuse toward the bonding layer more deeply with thicker oil layer on the substrate. The SEM micrograph and elemental distribution of the specimen covered with an oil layer thickness of 30 μm are shown in Figure 8(d). This indicated that the distribution range of Si increased to more than 100 μm. A large number of flaws and debonding features were found at the substrate–adhesive interface; this always reduced the shear strength and made the testing results more unpredictable.

Fracture Morphology Analysis

The fracture surface appeared to have different features because of the diversity of the sress distribution and bonding conditions after the shear failure. However, all of these fracture surfaces could be classified as the three basic models shown previously in Figure 1. The fracture surfaces of specimens covered with different oil layer thicknesses are shown in Figure 9, where the dimensions were all 25.4 $\times$ 12.7 mm^2. The bright areas in the figures are the aluminum substrate, and the dark areas are the remaining adhesive. This shows that all of the specimens ruptured according to model III, that is, the mixture of model I (cohesive failure model) and model II (interface failure model). However, the area ratios of models I and II showed great differences with increasing oil layer thickness. As shown in Figure 9(a), for the oil-free specimen, model I was the dominant failure model. The fracture surface showed a more uniform mophology than those of any other specimen. Under this failure model, the crack grew along the inside of the bonding layer. Moreover, as shown by the previous results, this kind of fracture morphology corresponds to a higher shear strength. Figure 9(b) shows the fracture surface of the specimen covered with an oil layer thickness of 10 μm. It presents a lower area ratio of model I and a rougher fracture surface than that of the oil-free specimen. When the oil layer thickness further increased [Figure 9(c,d)], model II became the dominant fracture model. Under this failure model, the crack grew along the substrate–adhesive interface, and it corresponded to the lower shear strength. These results are in accordance with the work of Seo and Lim,[29] in which the relationship between the failure strength and fracture surface morphology of adhesive-bonded joints was investigated. However, it is a pity that only a simple qualitative conclusion was obtained.

To further study the relationship between the fracture surface morphology and the shear strength, a comparison map was used to illustrate the correlation between the shear strength and cohesive failure area ratio of the fracture surface with different thicknesses of oil layers covering the substrate. As shown in Figure 10, although the results were not sufficient, the general tendency was still discernible. With increasing oil layer thickness, the cohesive failure area ratio decreased on the whole. Moreover, a larger distribution range and worse repeatability of the testing results were observed as well. It is noteworthy that the shear strength of the specimens covered with the oil layer thickness of 10 μm was only slightly lower than that of the oil-free specimens. However, their results distribution range was almost the same size. This phenomenon demonstrated that the 10 μm thick oil layer had little influence on the bonding reliability and performance reproducibility of the specimens. Therefore, the hybrid multiscale epoxy adhesive prepared in this study showed a capacity for bonding the oiled substrates.

CONCLUSIONS

The bonding performance and resulting distributions of a hybrid multiscale epoxy adhesive were investigated. The influence of the oil layer thickness on the shear strength, failure probability, and fracture surface morphology was investigated. Some important conclusions were drawn:

1. The shear strength of the oil-free specimens decreased with increasing bonding layer thickness, whereas it first increased and then decreased with increasing SCF content. The optimized bonding layer thickness and SCF content were 200 μm and 2 phr, respectively.
2. As the oil layer thickness increased, the shear strength decreased, whereas the distribution range of the testing results increased. The oil-accommodating adhesive developed in this study were used directly without degreasing when the oil layer thickness was smaller than 10 μm, where over 96% of the shear strength could be retained with almost changeless failure probability.
3. The oil diffused toward the bonding layer and thus formed an obvious interfacial feature at the substrate–adhesive interface. When the oil layer thickness was larger than 10 μm, excess oil at the interface reduced the shear strength sharply and thus worsened the bonding reliability and performance reproducibility of the bonded joints.
4. The failure model of the fracture surface was closely related to the testing results of shear strength. By analyzing the relevancy between the shear strength and cohesive failure area ratio, we found a novel correlation.

ACKNOWLEDGMENTS

The authors are grateful to Yinzhi Zhou for help with the specimen preparation and Weidi Dai for the use of SEM and EDAX instruments. The authors also express their sincere thanks to Xupu Yang for help with the shear test.

The authors contributed to this article in the following ways: conception and design, Zhongwei Zhang and Yefa Tan; financial support, Zhongwei Zhang and Yefa Tan; administrative support, Xiaolong Wang; provision of study materials or patients, Yefa Tan and Hua Tan; collection and assembly of data, Zhongwei Zhang and Xiang Hong; data analysis and interpretation, Zhongwei Zhang and Yefa Tan; manuscript writing, all authors; and final approval of the manuscript, all authors.

REFERENCES

1. Grant, L. D. R.; Adams, R. D.; da Silva, L. F. M. *Int. J. Adhes. Adhes.* **2009**, *29*, 535.
2. Pantelakis, S.; Tserpes, K. I. *Sci. China Phys. Mech.* **2014**, *57*, 2.
3. Markatos, D. N.; Tserpes, K. I.; Rau, E.; Markus, S.; Ehrhart, B.; Pantelakis, S. *Compos. B* **2013**, *45*, 556.
4. Kanakoudis, V. K.; Tolikas, D. K. *J. Water. Supply Res. Technol.* **2001**, *50*, 301.
5. Tupy, M.; Merinska, D.; Svoboda, P.; Kalendova, A.; Klasek, A.; Zvonicek, J. *J. Appl. Polym. Sci.* **2013**, *127*, 3474.
6. Siddaramaiah; Joy, V. A.; Gowri, A. N. S.; Leena, B.; Hemmige, V. V.; Deepa, S. *J. Appl. Polym. Sci.* **1998**, *68*, 2063.
7. Moffet, M. L.; La Saponara, V. *J. Appl. Polym. Sci.* **2013**, *130*, 3961.
8. Ogawa, T.; Hongo, M. *J. Adhes. Sci. Technol.* **1997**, *11*, 1197.
9. Debski, M.; Shanahan, M. E. R.; Schultz, J. *Int. J. Adhes. Adhes.* **1986**, *6*, 145.
10. Hong, S. G.; Boerio, F. J. *J. Adhes.* **1995**, *49*, 133.
11. Tang, L. C.; Wang, X.; Wan, Y. J.; Wu, L. B.; Jiang, J. X.; Lai, G. Q. *Mater. Chem. Phys.* **2013**, *141*, 333.
12. Zhang, G.; Rasheva, Z.; Karger-Kocsis, J.; Burkhart, T. *Express Polym. Lett.* **2011**, *5*, 859.
13. Zhang, G.; Karger-Kocsis, J.; Zou, J. *Carbon* **2010**, *48*, 4289.
14. Sharma, S. P.; Lakkad, S. C. *Surf. Coat. Technol.* **2010**, *205*, 350.
15. Chen, Q.; Zhang, L.; Zhao, Y.; Wu, X. F.; Fong, H. *Compos. B* **2012**, *43*, 309.
16. Kinloch, A. J.; Lee, J. H.; Taylor, A. C.; Sprenger, S.; Eger, C.; Egan, D. *J. Adhes.* **2003**, *79*, 867.
17. Ahmad, Z.; Ansell, M. P.; Smedley, D. *Int. J. Adhes. Adhes.* **2010**, *30*, 448.
18. Arronche, L.; La Saponara, V.; Yesil, S.; Bayram, G. *J. Appl. Polym. Sci.* **2013**, *128*, 2797.
19. Ma, H. Y.; Wei, G. S.; Liu, Y. Q.; Zhang, X. H.; Gao, J. M.; Huang, F.; Tan, B. H.; Song, Z. H.; Qiao, J. L. *Polymer* **2005**, *46*, 10568.
20. Zhang, H.; Zhang, Z.; Breidt, C. *Compos. Sci. Technol.* **2004**, *64*, 2021.
21. Kaynak, C.; Orgun, O.; Tincer, T. *Polym. Test.* **2005**, *24*, 455.
22. Ok, S.; Choe, Y. *Mol. Cryst. Liq. Cryst.* **2013**, *579*, 55.
23. Chang, L.; Zhang, Z.; Breidt, C. *Appl. Compos. Mater.* **2004**, *11*, 1.
24. Vietri, U.; Guadagno, L.; Raimondo, M.; Vertuccio, L.; Lafdi, K. *Compos. B* **2014**, *61*, 73.
25. Li, J.; Luo, R.; Bi, Y.; Xiang, Q.; Lin, C.; Zhang, Y.; An, N. *Carbon* **2008**, *46*, 1957.
26. Banea, M. D.; da Silva, L. F. M. *Proc. Inst. Mech. Eng. Part. L* **2009**, *223*, 1.
27. Russell, J. D. *SAMPE J.* **2007**, *43*, 26.
28. Ben Salem, N.; Bresson, G.; Jumel, J.; Shanahan, M. E. R.; Bellut, S.; Lavelle, F. *J. Adhes. Sci. Technol.* **2013**, *27*, 2278.
29. Seo, D. W.; Lim, J. K. *Compos. Sci. Technol.* **2005**, *65*, 1421.
30. Wilson, D. M.; Visser, L. R. *Compos. A* **2001**, *32*, 1143.
31. Chlopek, J.; Morawska-Chochol, A.; Bajor, G.; Adwent, M.; Cieslik-Bielecka, A.; Cieslik, M.; Sabat, D. J. *Biomater. Sci. Polym. Ed.* **2007**, *18*, 1355.
32. Zhang, Z.; Tan, Y.; Wang, X.; Tan, H.; Li, J. *Polym. Compos.* In press. DOI: 10.1002/pc.23125.
33. Jeenjitkaew, C.; Luklinska, Z.; Guild, F. *Int. J. Adhes. Adhes.* **2010**, *30*, 643.